Scientific Research Publishing

Materials Sciences and Applications, 2025, 16(4), 172-199
https://www.scirp.org/journal/msa
ISSN Online: 2153-1188
ISSN Print: 2153-117X

Physico-Chemical Analysis of African Hazelnut Shells "*Coula edulis*" from Cameroon

Eric Mbompouho Tchoffo[1,2*], Gilbert Tchemou[1,2], Elvis Mbou Tiaya[1,2*], Dieunedort Ndapeu[2,3], Michelle Dorense Yabia[1], Claude Takoumbe[1,2], Augustine Demze Nitidem[1,2], François Bayock Njock[1], Ebenezer Njeugna[1,2]

[1]Mechanical Laboratory, University of Douala, Douala, Cameroon
[2]Mechanics and Adapted Materials Laboratory, Higher Technical Teacher Training College, Douala, Cameroon
[3]Research Unit of Industrial Systems and Environmental Engineering (URISIE), UIT-FV Bandjoun, Cameroon, University of Dschang, Bandjoun, Cameroon
Email: erictchoffo49@gmail.com, elvistiaya@gmail.com

How to cite this paper: Tchoffo, M.E., Tchemou, G., Tiaya, E.M., Ndapeu, D., Yabia, M.D., Takoumbe, C., Nitidem, A.D., Njock, F.B. and Njeugna, E. (2025) Physico-Chemical Analysis of African Hazelnut Shells "*Coula edulis*" from Cameroon. *Materials Sciences and Applications*, **16**, 172-199.
https://doi.org/10.4236/msa.2025.164010

Received: February 2, 2025
Accepted: April 5, 2025
Published: April 8, 2025

Abstract

This work aims to characterize the physical, chemical, and thermal properties of hazelnut shells of the "*Coula edulis*" variety, originating from the south of Cameroon. The samples were divided into two zones (polar and equatorial) to study absorption and drying under four isotherms. The analyses allowed for the determination of the diffusion coefficient, the corrected diffusion coefficient, the relative humidity rate (RHR), and the activation energy using the gravimetric method. The results show that the relative humidity rate (RHR), of the polar region is higher than that of the equatorial region, while the diffusion coefficients and corrected diffusion gradually decrease. Among the models tested, the Page model best predicts humidity variations, while the Newton and Lewis models stand out for describing the drying phenomenon. "*Coula edulis*" has a dense structure with low porosity and limited water absorption, demonstrating their mechanical strength and dimensional stability. FTIR analysis highlights the presence of major lignocellulosic compounds (cellulose, hemicellulose, and lignin), while XRD reveals moderate crystallinity associated with mineral phases. ATG/DTG confirms good thermal stability up to high temperatures. These properties position the "*Coula edulis*" shells as a promising material for applications in bio-composites, thermal and acoustic insulation, or even as sustainable materials with a view to a circular economy.

Keywords

"*Coula edulis*", Thermal Properties, Absorption Kinetics, Activation Energy, Lignocellulosics

1. Introduction

The forests of Cameroon cover approximately 22.5 million hectares, which is 48% of the national territory [1]-[3]. In these forests, there are many species, some of which are little known to the public, notably the African hazel, which produces the "*Coula edulis*" hazelnut with seeds of great nutritional and therapeutic value [4]-[11]. Collected between June and September, these hazelnuts are a source of income for local populations [12]-[14]. The extensive exploitation of the African hazel tree is justified by the fact that these trees are present in very large numbers in the forest, and by the socio-economic importance of its fruits, almonds, and wood [15]-[18]. Some authors have studied the "*Coula edulis*" of Cameroon such as Chauvelin Douh *et al.* 2023 [19], they showed the potential for natural regeneration of some priority non-timber forest products in the Akom II production basin (South Cameroon) and they concluded that the African hazelnut is a species with low regeneration, from which it deserves to be protected. The "*Coula edulis*" hazelnut shell has a hard and woody shell that surrounds the nut, whose fruit is edible. It is about 2 cm in diameter and dark brown, its surface is smooth and slightly rough to the touch [20]. The shell of "*Coula edulis*" is composed of lignin and tannin, it also contains traces of minerals such as calcium, potassium, and magnesium [8] [9] [21] [22]. However, after extraction of the fruits, the waste of "*Coula edulis*" (3902 tons per year) is abandoned in nature, thus polluting the environment and gradually degrading by adsorbing water [23] [24]. Certain plant husks are often eliminated by open-air combustion and toxic gases are emitted during this combustion. Which can harm human health and the environment, [25]-[27]. Several authors have dedicated themselves to working on the characterization of plant shells, such as Madhiyanon *et al.* 2009, Isa and Jimoh 2021, Sahari *et al.*, 2023 [28]-[30] worked on the use of models for the phenomenon of drying thin layers of coconut shells. They show from an analysis of statistical parameters that the Henderson and Pabis model, the Page model, and the Peleg model best satisfy the change in humidity. Ndapeu *et al.* 2013, worked on an Experimental Study of the Drying Kinetics of the Coconut Shells (Nucifera) of Cameroon [31]. The analysis of statistical parameters shows that the Midilli model best predicts this drying phenomenon. The corrected diffusion coefficient was determined at different temperatures which allowed the evaluation of the activation energy from the Arrhenius equation. Ndapeu *et al.* 2016, and Ganou *et al.* 2020, worked on the theory of water diffusion and the microstructure of coconut shells (Nucifera) and the cores of *Canarium schweinfurthii*, [32] [33]. The results from the analysis of their work showed that the absorption rate of *Canarium schweinfurthii* (CS) is greater than that of coconut Nucifera shells (CN). The corrected diffusion coefficient and the activation energy of *Canarium schweinfurthii* (CS) are lower than the activation energy of coconut Nucifera shells (CN). The characteristics of hardcore vegetable shells show that they can be used as filler composites [34]-[36]. Concerning hazelnut shells, some researchers have used them in the production of activated carbon. Mexcent Zue Mve *et al.* 2020, prepared and characterized ac-

tivated carbons obtained from the shells of "*Coula edulis*" nuts [37]. The kinetic study showed that the adsorption reactions of Magnesium ions are proportional to the product of the concentrations of the available absorption sites. Whereas that of humic substances depends solely on the concentration of a single reagent and is characterized by an external mass transfer mechanism. Beyegue *et al.* 2023 worked on the evaluation of the acute and subchronic toxicity of the ethanolic extract of "*Coula edulis*" (Olacaceae) [38]. The results show that the plant can be recommended without risk for therapeutic use. Given the literature, no physico-chemical and thermal characterization has been carried out on the shells of "*Coula edulis*". The objective of this work is to contribute to the valorization of biomass from the shells of "*Coula edulis*", applying the theory of diffusion to evaluate its activation energy.

2. Material and Methods

2.1. Hazelnut Shell Supply

The African hazelnut shells "*Coula edulis*" subjected to the study were collected in the South region of Cameroon, Ocean Division, and more precisely in the village of Kribi. They were subsequently transported to the University of Douala (ENSET of Douala) specifically to the Mechanical Engineering Department. **Figure 1** shows the nuts of "*Coula edulis*" and **Figure 2** shows the cross-section of the different areas of the shell.

Figure 1. The nuts of "*Coula edulis*" (*Coula edulis*).

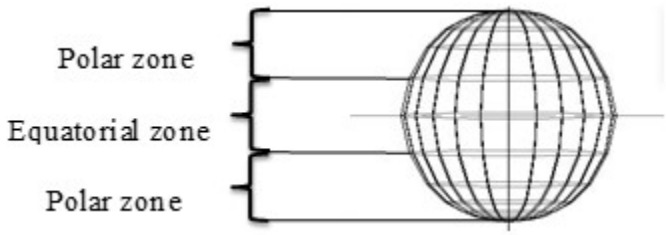

Figure 2. Cross section of the different areas of the shell.

2.2. Zone distinction

To continue this work, two zones of the hulls were identified based on the literature by Ganou *et al.* 2020 [33], namely: the equatorial zone (E) and the polar zone (Po), which were labeled according to the different zones before the testing phase. **Figure**

3. presents the principle of distribution of the different extraction zones.

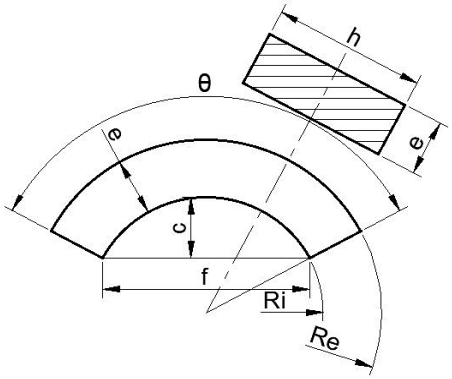

h: sample height; e: sample thickness; R_i: Inner radius; R_e: External radius; f: chord to the inner circle; c: sample curvature; θ: angle of curvature.

Figure 3. Shape of a sample.

2.3. Physical Characterizations of "*Coula edulis*" Shells

2.3.1. Drying Study

The samples (**Figure 4(a)**) are taken manually in the zones (equatorial and polar) [33]. The samples are weighed (**Figure 4(b)**) with a balance to the nearest hundredth of a gram, to measure the mass and introduced into the Memmert UF110 incubator (**Figure 4(c)**).

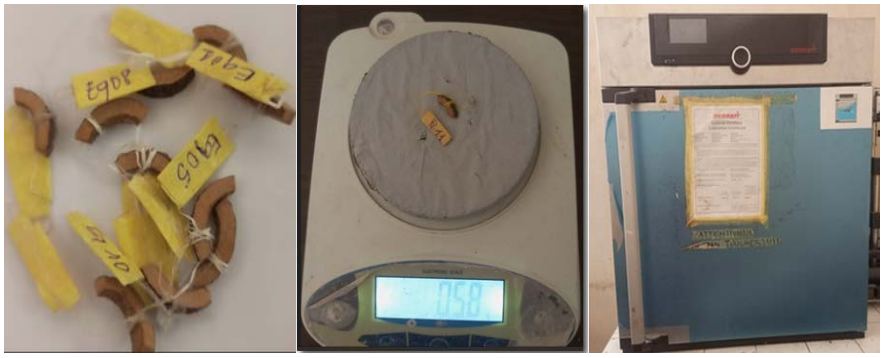

(a) (b) (c)

Figure 4. Description of the sample (a) Equatorial zone samples; (b) Digital balance precision 0.01g; (c) Memmert UF110 incubator.

The drying was carried out using a gravimetric method [39] [40]. This method consists of a cycle of mass gain repeated at regular time intervals until a constant mass is obtained. The test begins with short time intervals which are gradually increased until total stability is achieved. The choice of the four isotherms (60˚C, 75˚C, 90˚C, 105˚C) in a study on the drying kinetics of *Coula edulis* shells can be justified by considering several scientific and technical aspects, including the effect of temperature on water diffusion:

At 60˚C and 75˚C, water removal occurs mainly by slow diffusion through the

porous matrix.

At 90˚C and 105˚C, drying becomes faster because thermal energy further accelerates water migration to the surface. Comparison of these temperatures allows us to assess whether drying is limited by internal diffusion or by surface evaporation. These temperatures are generally used in the literature for similar biomaterials [31] [33] [41] (walnut shells, plant fibers) to obtain comparable drying models. They allow the application of mathematical models (drying isotherms, Arrhenius law, etc.) to estimate drying parameters, such as the activation energy of the process. Thus, the choice of temperatures 60˚C, 75˚C, 90˚C and 105˚C therefore makes it possible to exploit the balance between loading efficiency and preservation of shell properties. Equation (2) made it possible to find the mass loss rate which is a unitless quantity (MR).

$$\mathrm{THR} = \left(\frac{M_h}{M_S} - 1\right) \times 100 \tag{1}$$

$$\mathrm{MR} = \frac{M_t - M_S}{M_h - M_S} \tag{2}$$

where THR(%) is the moisture content; M_h is the mass of the sample in the humid state (g); M_S is the mass of the sample in the anhydrous state (g); M_t is the mass at each instant (t); MR is the mass loss rate. Some mathematical model equations of the drying kinetics are observed in the literature and presented in **Table 1** [1] [28]-[30] [42].

Table 1. Some models of drying kineti.

Auteurs	Mathematical models	Parameters	References
Newton and Lawis	$f(t) = a\exp(-k*t)$	01	
Page	$f(t) = a\exp(-k*t^n)$;	02	
Henderson and Pabis	$f(t) = a*\exp(-k*t)$		
Logarithmic	$f(t) = a*\exp(-k*t)+b*t$	03	
Midilli	$f(t) = a*\exp(-k*t^n)+b*t$	04	[28] [41]-[44]
Verma and al	$f(t) = a*\exp(-k*t)+(1-a)*\exp(-g*t)$	03	
Anderson and Pabis Modifié	$f(t) = a*\exp(-k*t)+b*\exp(-g*t)+c*\exp(-h*t)$	06	
Peleg	$f(t) = 1-\left[t/(a+b*t)\right]$	02	
Aghbashlo	$f(t) = \exp\left(-k*t/(1+a*t)\right)$	02	

a, b, g, k, h and n represent model parameters; t represents drying time (minutes).

The chosen model is the one that presents a correlation coefficient close to unity 1 (R^2), the lowest Root Mean Square Error (RMES), and the smallest model parameters. The diffusion coefficient in drying is calculated using Equation (3) and a corrected diffusion coefficient is applied to globally integrate the geometry of the material (**Figure 3**). This corrected diffusion coefficient is calculated with Equation (4).

$$D_{eff} = \frac{4 \times k \times e^2}{\pi^2} \tag{3}$$

$$D_{ceff} = D_{eff} \times \left(1 + \frac{e}{L} + \frac{e}{l}\right)^{-2} \tag{4}$$

Where D_{eff} is the diffusion coefficient ($m^2 \cdot s^{-1}$); k is the slope of the linear part obtained experimentally according to works from the literature [29] [42]; D_{ceff} ithe corrected difusion coefcient; ($m^2 \cdot s^{-1}$); L is the length of the sample (m); l is the width of the sample in (m); e is the thickness of the sample along the difusion axis (m). The thickness and length of the sample (**Figure 3**) were determined from the respective Equations (5) and (6).

$$e = R_{ext} - R_{int} \tag{5}$$

$$L = \frac{\pi \cdot R_a \cdot \theta}{180} \tag{6}$$

Where R_{ext} is the external radius (m), R_{int} is the inner radius (m), R_a: Average radius (m); θ: Central angle (rad). In this equation, k is the slope of the linear part, determined by the function $\ln \mathrm{MR} = f(t)$. The activation energy is a characteristic factor of the diffusion phenomenon [29] [30], it is determined using the Arrhenius Equation (10).

$$D_{eff} = D_0 \exp\left(-\frac{E_a}{RT}\right) \tag{7}$$

Where R is the perfect gas constant (8.314 J/mol/˚K); T is the absolute temperature of the drying chamber in Kelvin (˚K); D_o is the Arrhenius constant in (m^2/s); E_a: is the activation energy in (KJ/mol). The logarithmic transformation of Equation (7) gives the following equation:

$$\ln\left(D_{eff}\right) = \ln\left(D_0\right) - \frac{E_a}{R} \times \frac{1}{T} \tag{8}$$

The values of the diffusion coefficient calculated by the different experiments are plotted as a function of $1/T$ where the slope of the line is defined by Equation (9) with E_a defined by the Equation (10).

$$D = \frac{a}{T} + b \tag{9}$$

$$E_a = -a \times R \tag{10}$$

Where E_a is the activation energy.

2.3.2. Study of the Water Absorption Phenomenon

The geometry of the samples is the same as in the drying study (**Figure 4(a)**). Seven samples per zone, for a total of fourteen previously dried in an oven at 105˚C for three hours. These samples are attached to 10 g mass nuts, the whole (sample + nut) after immersion in distilled water is placed back in the oven for 30 minutes to remove excess moisture. This rapid drying helps stabilize the sample and prepare for more accurate measurements of its mass. The whole is weighed and the initial mass is recorded (Mi). Subsequently, the whole is immersed in distilled water at room

temperature. A weighing cycle at regular time intervals using a scale to the nearest hundredth of a gram (**Figure 4(b)**) is used until a constant mass is obtained. This method is used by several authors in the literature [39] [40]. The absorption rate (W%) was calculated from the relationship Equation (11), and the absorption ratio (MR) which is a unitless value was calculated from Equation (12).

$$W(\%) = \left(\frac{M_f}{M_i} - 1\right) \times 100 \tag{11}$$

$$\mathrm{MR} = \frac{M_t - M_i}{M_f - M_i} \tag{12}$$

Where W is the absorption rate (%); M_f is the mass of the sample saturated with water (g); M_i is the mass of the sample in the anhydrous stat (g); M_t is the ms of the sample at the time of analysis (g); MR is the ratio. The equation of the slope k is determined from the function $\ln(1-\mathrm{MR}) = g(t)$ [45].

As a result, some mathematical models of absorption kinetics are retained in the literature and presented in **Table 2** [33] [45] [46].

Table 2. Some absorption models.

Auteurs	Mathematical models	Parameters	References
Czel and Czigany	$g(t) = a * t^m$	01	[32] [33] [45]-[47]
Page	$g(t) = 1 - a * \exp(-k * t^n)$	03	
Mohsenin	$g(t) = a * [1 - \exp(-k * t)] + c * d * t$	04	
Gowen	$g(t) = (a - b) * \exp(-k * t) + b$	04	
Sikame	$g(t) = c - a * \exp(-k * t) - b * \exp(-m * t)$	05	

a, b, c, k, m and n represent model parameters; t represents absorption time (minute).

2.3.3. Determination of Porosity Rate

According to the ISO 3344 standard, the powder from the "Coula edulis" shells of each sampling area was used to fill two 20 ml bottles. This powder is introduced into the oven and maintained at a temperature of 105˚C ± 3˚C for 24 hours. Then they are weighed. m_0 (Anhydrous mass) on a laboratory balance with a precision of 0.01 g. The pycnometer is then filled with demineralized and degassed water up to the zero of the meniscus, and the whole is stabilized at the reference temperature before being weighed m_1. Part of the water contained in the pycnometer is emptied and the mass m_0 of sample is introduced. The water level is adjusted using a pipette up to the zero of the meniscus. The assembly is stabilized and then weighed to obtain the mass m_2. Surface water is removed using a filtration/absorption system; then the sample is weighed and the mass m_3 is obtained. Relation (13) was used to calculate the apparent density. The real density is determined by the gravimetric method based on the displacement of the water column following the literature work. The real density was calculated using Equation (14).

$$\rho_{app} = \frac{m_0 \times \rho_{eau}}{m_3 + m_1 - m_2} \tag{13}$$

$$\rho_{abs} = \frac{m_0 \times \rho_{eau}}{m_0 + m_1 - m_2} \tag{14}$$

Thus, Equation (15) gives us the calculation of porosity.

$$v = \frac{\rho_{abs} - \rho_{app}}{\rho_{abs}} \times 100\% \tag{15}$$

Where v (%) is the porosity; ρ_{abs} (g/cm^3) is the real density; ρ_{app} (g/cm^3) is the apparent density; ρ_{eau} is the density of the water(1000 g/cm^3); m_0 (g) is the mass of a sample dried in the oven; m_1 is the mass of the Chatelier pycnometer fcilled with water up to the Gauge line; m_2 is the mass of the Chatelier pycnometer containing the sample and water up to the gauge mark after 24 h of immersion in the water bath; m_3 is the mass of the superficially dry saturated sample.

2.4. Chemical and Thermal Characterizations Of Hazelnut Shells

2.4.1. Fourier Transform Infrared (FTIR) Spectrometry

Fourier Transform Infrared spectrometry (FTIR) made it possible to analyze the functional groups present in the shell of "*Coula edulis*" based on the characteristic vibrations of chemical bonds. This analysis is done using a Thermo Fischer USA, at room temperature and over a wavelength from 4300 cm^{-1} to 300 cm^{-1}.

2.4.2. Thermogravimetric Analysis (TGA)

Thermogravimetric Analysis (TGA) is performed on powders derived from the shells of "*Coula edulis*" using a TGA Q500 V20 universal device. The samples are subjected to a temperature range from 30˚C to 1000˚C. The heating rate is imposed at 10˚C/min. The test is conducted under nitrogen (N2). This analysis allows for the determination of the moisture content, the thermal stability temperature of the material, as well as the degradation temperature.

2.4.3. X-Ray Diffraction (XRD)

An XRD analyzer (Bruker D2 phaser XDR), operating in reflection mode (Cu, Kα), was used. The scans are 0.5 min^{-1}. The software for processing DRX analysis data files made it possible to identify the different phases, with the "Crystalography Open Database".

3. Results and Discussions

3.1. Physical Characteristics

3.1.1. Drying Study

The results obtained for the relative humidity rate (RHR) in the polar zone are 16.05% ± 2%. As for the equatorial zone, the relative humidity rate is 13.38% ± 3%. The results obtained are presented in **Figure 5**. The values obtained are close to certain shells known in the literature, notably Nucifera coconut shells from Cameroon (15.5%), and also lower than certain other shells such as *Canarium*

schweinfurthii kernels (14%) [31] [33]. The observation of the results obtained in Figure 5. Shows that the relative humidity rate in the polar zone is higher than that in the equatorial zone. This can be explained by the fact that the equatorial zone of the "*Coula edulis*" has a higher evaporation, which reduces the relative humidity rate, unlike polar zones.

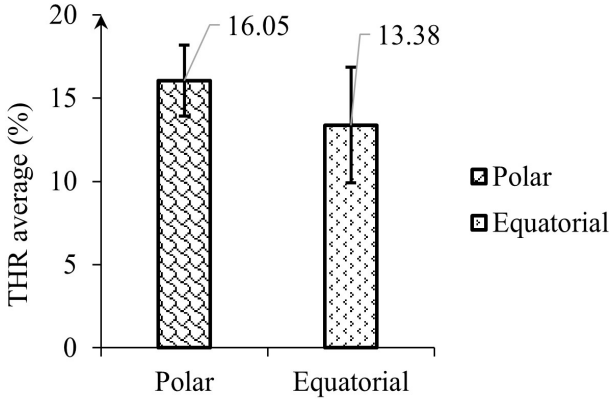

Figure 5. Distribution curve of relative humidity rates.

As for the drying kinetics, the different experimental points obtained from equation (2) are modeled in the Matlab R2010a environment. It can be seen from Figure 6 that the drying kinetics curves are similar for the polar zone and the equatorial zone. This is observed in the literature on other materials [41]. The "Experimental points" curve (blue stars) represents the data observed during drying. Theoretical models (Newton and Lawis, Page, Henderson and Pabis,

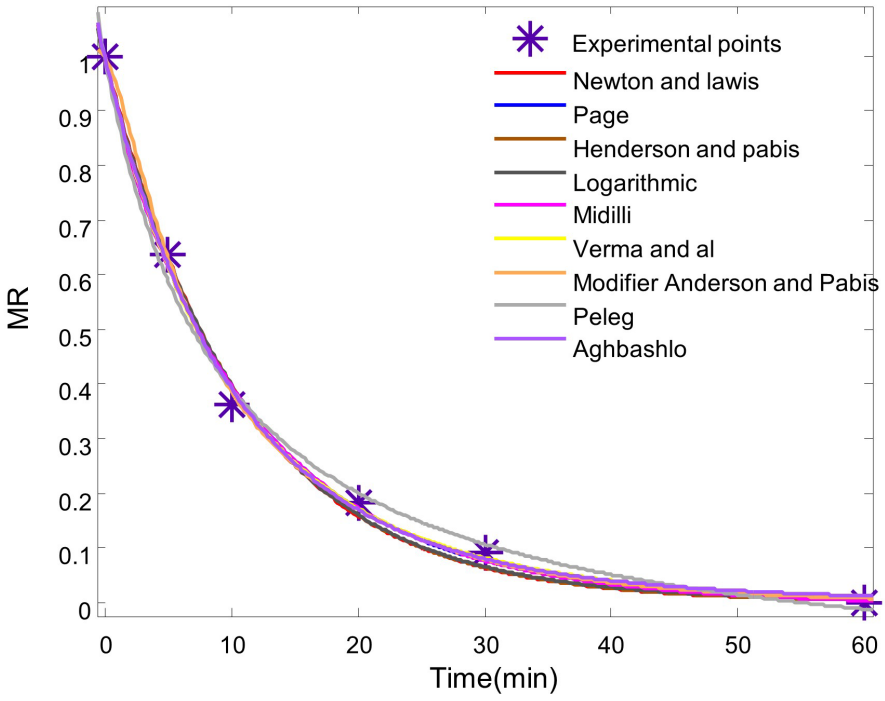

Figure 6. Simulated model of the drying kinetics of a sample from the polar zone.

Logarithmic, Midilli, Verma *et al.*) aim to fit the experimental data. Among these models, some seem to fit the experimental points better than others, notably the Newton and Lawis model and the Logarithmic model, which are closer to the experimental points. The decrease in relative humidity (MR) content with time follows a decreasing exponential curve, typical of drying processes. Models like Midilli and Page show reasonable approximations, but deviations from experimental data can be seen. Complex models like Newton and Lawis or Aghbashlo include more adjustable parameters, which may explain their better correlation with real data.

In the literature, the drying kinetics of other plant shells, such as coconut, palm, or shea shells, show similar curves. However, the differences lie in: Shell density and structure: Denser shells retain moisture longer, slowing down drying [42]. Drying conditions, temperature, relative humidity, and air velocity influence the kinetics. For example: Coconut shells show kinetics close to the Page model, due to their high porosity. Palm shells often approach the Logarithmic and Midilli models, due to a less dense structure. The Midilli model, with its good fit, could be recommended to predict the drying behavior of *Coula edulis*. Compared to other plant shells, *Coula edulis* appears to have a relatively fast drying curve, probably due to its specific composition and low resistance to moisture diffusion. This could have implications for the optimization of industrial drying processes, by adjusting parameters to minimize processing time and save energy. Table 3 presents the parameters of the Newton-Lewis model for the two zones and the four isotherms obtained from Table 1.

Table 3. Drying kinetics model parameters.

Models	Parameters	Temperatures	Polar zone		Equatorial zone	
			R^2	K	R^2	K
Newton and Lawis	01	60˚C	0.996	0.097	0.995	0.095
		75˚C	0.994	0.095	0.997	0.093
		90˚C	0.995	0.093	0.997	0.093
		105˚C	0.994	0.096	0.995	0.095

Figure 7 shows that the drying kinetics model is faster at higher temperatures, consistent with the expected physical behavior. At 105˚C, the relative moisture (MR) content decreases very rapidly compared to lower temperatures. At 60˚C, drying is slower, indicating little moisture diffusion. At all temperatures, the Newton and Lewis model fits the experimental points well, although some deviations are observed, particularly at high MR (early drying). This can be explained by the simplified nature of the model. The discrepancy is more pronounced at low temperatures (60˚C), where diffusion and internal resistance effects may be more important, exceeding the assumptions of the Newton model. The effect of temperature is visible: increasing the temperature accelerates the drying process,

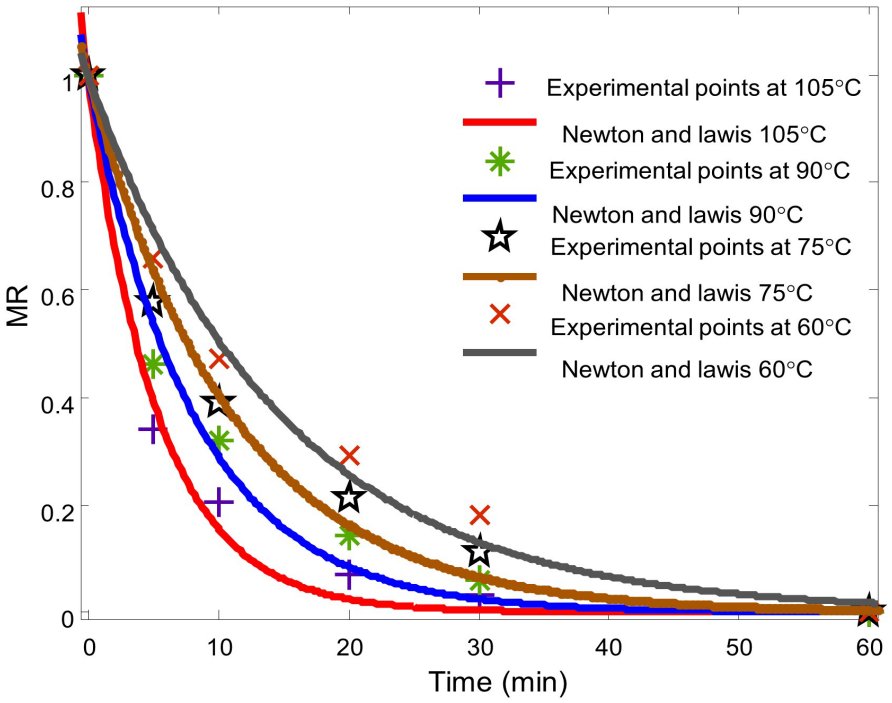

Figure 7. Presentation of the Newton and Lawis model on drying kinetics.

reducing the time needed to reach low relative humidities. The Newton and Lewis model is found to be robust in capturing general drying trends at different temperatures, although more complex models could fit the data better. In the literature, the Newton model is commonly used for materials with low structural complexity, such as thin fruits, seeds, or light shells. Studies on plant shells such as coconut, peanut, or palm show that the Newton model gives similar fits for high temperatures (>90˚C) but tends to underestimate internal phenomena at low temperatures. The Newton and Lewis model provides a fast and efficient approximation to analyze data from drying of *Coula edulis*. Compared to work on other plant shells, *Coula edulis* appears to have faster drying kinetics, perhaps due to its specific porous structure or low thickness. The diffusion coefficient is obtained after drying of the samples and is determined from equation (4). The average values obtained range from 1.27E−07 ± 1.13E−08 (m^2/s) to 2.35E−07 ± 1.17E−08 (m^2/s) and from 1.24E−07 ± 9.83E−09 (m^2/s) to 1.52E−07 ± 1.28E−08 (m^2/s) for the isotherms of 60˚C, 75˚C, 90˚C and 105˚C. [43]. The values of the diffusion coefficient are reported in **Table 4** as well as those of the corrected diffusion coefficient. **Table 4**: Synthesis of diffusion coefficients.

Table 4. Synthesis of diffusion coefficients.

		Polar		Equatorial	
		Deff ($m^2 \cdot s^{-1}$)	Deffc ($m^2 \cdot s^{-1}$)	Deff ($m^2 \cdot s^{-1}$)	Deffc ($m^2 \cdot s^{-1}$)
105°C	Average	2.35E−07	4.82E−08	1.52E−07	3.86E−08
	Ecartype	1.17E−08	4.89E−09	1.28E−08	3.27E−09

Continued

90°C	Average	1.46E−07	3.87E−08	1.32E−07	3.61E−08
	Ecartype	1.20E−08	4.30E−09	8.07E−09	1.69E−09
75°C	Average	1.42E−07	3.62E−08	1.27E−07	3.43E−08
	Ecartype	9.14E−09	2.33E−09	1.13E−08	3.05E−09
60°C	Average	1.21E−07	3.07E−08	1.24E−07	3.26E−08
	Ecartype	1.20E−08	2.49E−09	9.84E−09	3.24E−09

Figure 8, Shows that the corrected diffusion coefficient evolves in a decreasing manner with the evolution of the temperature. The corrected diffusion coefficient increases with temperature, which is expected since diffusion is favored by higher temperatures. This is related to the increase in kinetic energy of water molecules and the decrease in viscosity of water in the pores of the material. The values for the polar regions are systematically slightly higher than those for the equatorial regions, independent of the temperature. This suggests a structural or textural difference between these two areas of the sample (e.g., the porosity or density could be higher in the polar region, facilitating increased diffusion). At 105˚C: The diffusion coefficient is the highest (5.5×10^{-8} m^2/s for the polar region and 5×10^{-8} m^2/s for the equatorial region). This is expected because high temperatures promote rapid evaporation and faster diffusion. At 90˚C: A slight decrease is observed compared to 105˚C (4.5×10^{-8} m^2/s for the polar region and 4×10^{-8} m^2/s for the equatorial region). This indicates a strong temperature dependence of the diffusion coefficient in this range. At 75˚C and 60˚C: The corrected diffusion coefficients continue to decrease, reaching their lowest values (2.5×10^{-8} m^2/s at 75˚C and 2×10^{-8} m^2/s at 60˚C). This is related to the reduction of thermal energy available for the movement of water molecules. The differences between the polar and equatorial regions can be attributed to: A more porous structure or more permeable material in the polar region. A non-homogeneous distribution of initial moisture. These structural variations may influence the ability of water to diffuse in each region. The increase in the diffusion coefficient with temperature is consistent with diffusion theory, where the diffusion coefficient is exponentially related to temperature (Arrhenius law). The corrected diffusion coefficients (10^{-8} m^2/s) are consistent with results reported for similar materials (seeds, plant hulls) [33] [44]. These results can be used to optimize the industrial drying of *Coula edulis* hulls. A high drying temperature (90˚C - 105˚C) could be recommended to minimize drying time, although this must be balanced with energy costs and the risk of thermal degradation.

Observation of the curve in Figure 9 indicates a very good correlation between the experimental data and the Arrhenius model ($R^2 = 0.9669$). The negative slope shows that the effective diffusion decreases with the inverse of the temperature (which corresponds to an increase of Deff with temperature). The activation energy is 9.924 $kJ \cdot mol^{-1}$ for the equatorial zone and 3.917 $kJ \cdot mol^{-1}$ for the polar zone.

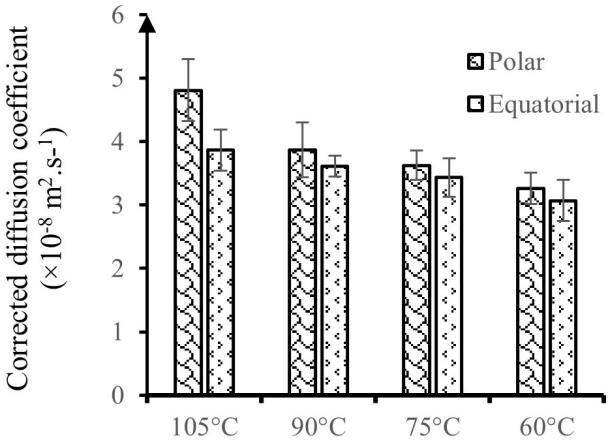

Figure 8. Distribution curve of the diffusion coefficient.

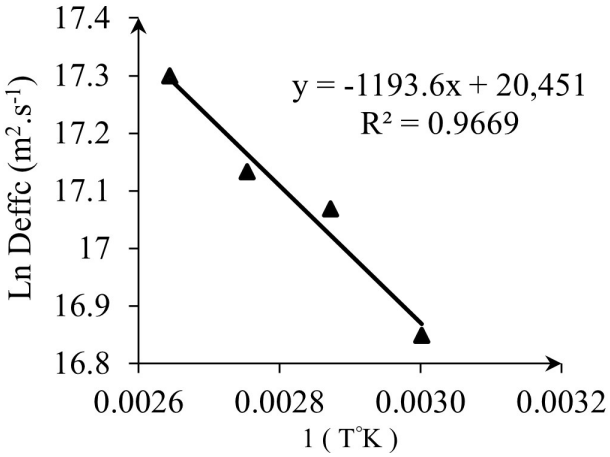

Figure 9. Arrhenius curve.

This suggests that the diffusion of water in the sample is mainly controlled by physical mechanisms such as migration in pores or capillarity. Compared to other plant materials, this value is in the expected range (8 - 30 kJ/mol), indicating a moderate ease of water migration under the effect of temperature. Studies on similar products, such as seeds or vegetable shells. [43] report similar values. This analysis confirms that the Arrhenius model is well suited to describe the effect of temperature on the diffusion coefficient during the drying of *Coula edulis* shells. The results obtained make it possible to effectively predict the drying behavior at different temperatures and to optimize industrial conditions. **Table 5** compares the data obtained with those in the literature.

Table 5. Comparative drying analysis.

	Cocos nucifera (CN) (Species 1)	*Cocos nucifera* (CN) (Species 2)	*Canarium schweinfurthii* (CS)	*Coula edulis* (CE)	
				Polar	Equatorial
Temperature (°C)	70 - 180		50 - 90	60 - 105	
Model of drying kinetics	Midilli		Page	Newton and Lawis	

Continued

Deff (m^2/s)	Min	1.46×10^{-8}	1.34×10^{-8}	2.70×10^{-11}	1.24×10^{-7}	2.35×10^{-7}
	max	16.10×10^{-8}	24.50×10^{-8}	39.00×10^{-11}		
Ea ($KJ.mol^{-1}$)		31.69	34.46	28.66	3.917	9.924
Reference		[28]	[31]	[33]	Case studied	

It is observed from **Table 5** that the temperatures used for *Cocos nucifera* are higher, which may be related to its denser structure requiring more energy to evacuate water. The moderate ranges for *Canarium schweinfurthii* and *Coula edulis* indicate a different behavior in terms of drying kinetics, probably due to higher porosity or better internal diffusion. The choice of the model indicates that *Cocos nucifera* has more complex nonlinear drying curves than the other species. Simple models (Page, Newton and Lewis) are sufficient to represent the drying behaviors of *Canarium schweinfurthii* and *Coula edulis*, suggesting uniform diffusion and a smooth response to temperature. *Coula edulis* shows much higher diffusion coefficients than the other two species, reflecting a faster and more efficient water extraction under the effect of temperature. The lower values for *Canarium schweinfurthii* could be attributed to a denser matrix or stronger interactions between water and shell components. The activation energy for *Coula edulis* is much lower than for the other two species. This shows that *Coula edulis* requires less energy for water to diffuse, which is consistent with its higher diffusion coefficients. *Cocos nucifera* and *Canarium schweinfurthii* have similar *Ea*, indicating more demanding drying mechanisms. In comparison with recent literature, studies on other shells such as peanut seeds or palm shells generally show *Ea* between 10 - 40 kJ/mol. [28] [33]. The values obtained for *Coula edulis* are distinguished by their low *Ea*, which could indicate a different chemical composition or a more favorable porous structure. These observations confirm the variability of drying properties depending on the structure and composition of plant shells.

3.1.2. Study of Water Absorption

The results obtained show that the water absorption rate is 16.32% ± 3.20% in the polar zone and 18.47% ± 2.04%. The results obtained are presented in **Figure 10**. The values obtained are lower than some hard-core plant shells known in the literature, notably the kernels of *Canaruim schweinfurthii* (30.13%) [32] [33], coconut shells (Nucifera) (17.32% ± 1.06%) and (20.42% ± 1.94%). Observations of the results obtained showed that the average absorption rate of the polar zone is lower than that of the equatorial zone. This can be justified by the colder temperature of the polar zone slowing down the process of absorption of the shell of "*Coula edulis*". On the other hand, the temperature in the equatorial zone favors faster absorption (**Figure 10**).

Regarding water absorption, the different experimental points obtained from Equation (12) are used in the Matlab R2010a environment. **Figure 11** shows the

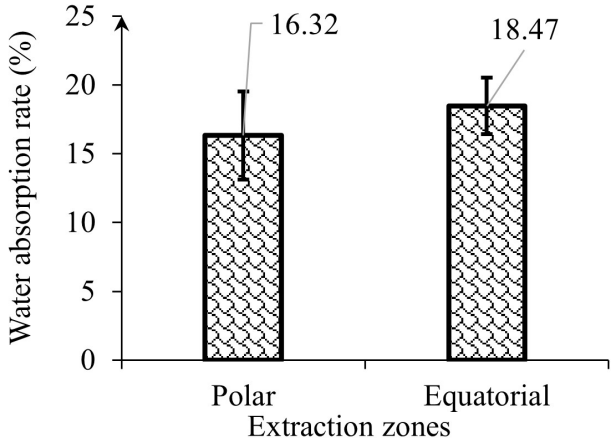

Figure 10. Absorption rate distribution.

different models simulated on the experimental points of a sample from the equatorial zone. The experimental points illustrate the kinetics of water absorption expressed by the relative humidity ratio (MR) as a function of time. The data show a rapid increase in humidity (MR) in the early phases, followed by a stabilization around MR = 1, indicating a steady state. The simulated models of Sikame and Page provide a precise fit over the entire curve, with predictions close to the experimental points, particularly in the initial and steady-state phases [33] [46]. The Gowen model shows an acceptable fit but tends to underestimate the intermediate MRs (0.2 - 0.6). The Czel_Czigany model largely overestimates the intermediate MRs and shows a generally poor fit. The Mohsenin model shows a poor fit, particularly in the initial and intermediate phases. The comparative analysis shows several phases: the initial phase (<500 min): The Sikame and Page models align well with the experimental points, indicating that they better capture the rapid absorption kinetics.

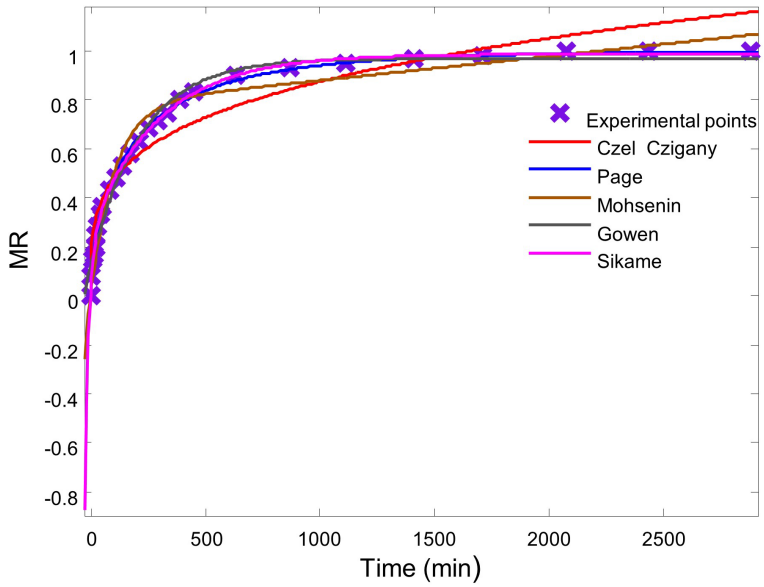

Figure 11. Simulated model of the absorption kinetics of a sample from the equatorial zone.

The other models (Czel_Czigany and Mohsenin) show discrepancies, reflecting an inability to correctly describe the early stages of rapid hydration. Intermediate phase (500 - 1500 min): Sikame and Page remain consistent with the experimental points. Czel_Czigany and Mohsenin overestimate the relative humidity, indicating an inaccuracy in the description of the partial equilibrium mechanisms. And the Equilibrium phase (>2000 min): All models, except Mohsenin and Czel_Czigany, converge towards the experimental values, showing their ability to correctly model saturation. Sikame and Page are frequently cited for their accuracy in modeling tropical products. For example, studies on similar shells (*Canarium schweinfurthii* and *Cocos nucifera*) have shown similar performance [33]. The dense and hydrophobic structure of *Coula edulis* shells may explain the slow absorption kinetics. Models such as Sikame, which take these parameters into account, are more accurate [45]. Sikame and Page show a high coefficient of determination (R^2) in several comparative studies, confirming their effectiveness in predicting hydration kinetics for similar nut or seed shells. Best Models: Sikame and Page show the best overall fits to experimental data and are confirmed by recent work on similar products. The Czel_Czigany and Mohsenin models are not suitable for *Coula edulis* shells, requiring adjustments or reformulations to improve their accuracy. **Figure 12** presents the representation of the Page model simulated on a sample of the equatorial zone. **Table 6** presents the parameters of the constants of the Page model for the two zones.

Table 6. Water absorption model parameters.

Model	N° Samples	Zone polar				Zone equatorial			
		R^2	K	n	a	R^2	K	N	A
Page	1	0.9965	0.1886	0.4838	0.9881	0.9824	0.2677	0.4037	1.0220
	2	0.9920	0.1196	0.4945	1.0210	0.9978	0.0400	0.6697	1.0150
	3	0.9880	0.0758	0.5702	1.0520	0.9993	0.0284	0.7526	1.0060
	4	0.9976	0.0338	0.6075	1.0300	0.9988	0.0445	0.6777	1.0060
	5	0.9955	0.0032	1.0990	0.9645	0.9928	0.0886	0.4577	1.0300
	6	0.9977	0.0299	0.6819	0.9937	0.9979	0.0191	0.7197	1.0190
	7	0.9986	0.0332	0.6906	0.9951	09983	0.0341	0.6396	0.9945

In **Figure 12**, the experimental points closely follow the curve simulated by the Page model, with excellent fit over the entire time range. This performance reflects a precise fit, validated by a high coefficient of determination (R^2) in many similar studies. The different phases of water absorption are observed: Initial phase (<500 min): The model perfectly describes the rapid water absorption by the shells, capturing the steep slope at the beginning of the curve. This stage is influenced by porosity and the availability of hydrophilic sites. Intermediate phase (500 - 1500 min): The transition to an equilibrium state is well represented, with a progressive stabilization of the curve. Equilibrium phase (>2000 min): The model effectively predicts saturation, re-

flecting the achievement of water equilibrium. Positioning to the literature, The Page model is recognized for its simplicity and efficiency in modeling mass transfer processes, particularly for structures such as nut and seed shells. Recent work [33] [45] has shown that the Page model provides superior fits for similar products, with R^2 often above 0.98. The dense and semi-permeable structure of *Coula edulis* shells influences their absorption kinetics, making adapted models such as Page essential to capture these dynamics. Compared to other models (Czel_Czigany, Mohsenin), Page better integrates the exponential curvature observed in the initial phases. Studies on *Cocos nucifera* and *Canarium schweinfurthii* show that the Page model is frequently used for similar lignocellulosic matrices, with consistent results (high R^2, low root mean square error). The Page model is simple, accurate, and applicable to a wide range of biological products. Effectively captures all three phases (rapid absorption, transition, equilibrium) of absorption kinetics. Valid for similar shells, as confirmed by recent work in the literature [33] [45]. **Table 7** positions the results found to those of the literature.

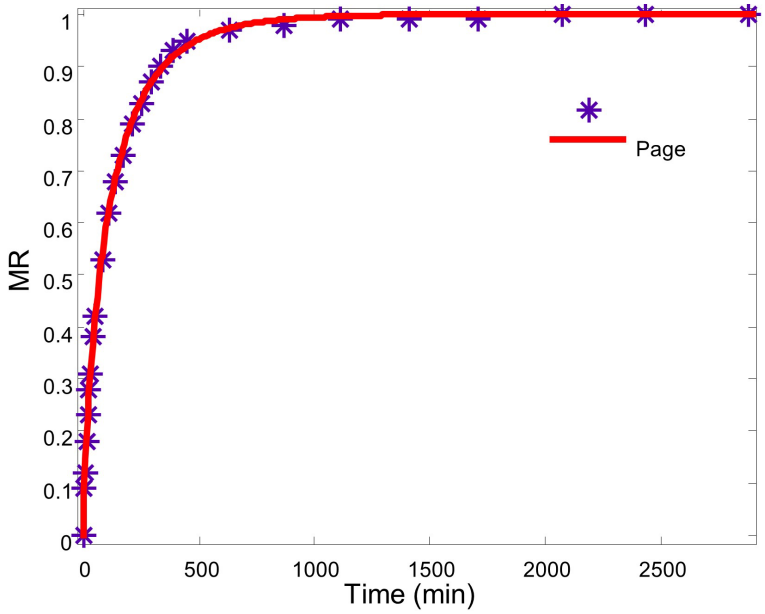

Figure 12. Presentation of the Page model on water absorption kinetics in the Equatorial zone.

Table 7. Presents the results of adsorption kinetics in comparison with the shell of coconut nucifera (CN).

	Cocos nucifera (CN) (Species 1)	*Cocos nucifera* (CN) (Species 2)	*Coula edulis* (CE)	
			Polar	Equatorial
Water absorption model		Page		
W (%)	17.32 ± 1.06	20.42 ± 1.95	16.32 ± 3.2	18.47 ± 2.2
Reference		[33]	Case studied	

Coula edulis shells exhibit different water absorption rates depending on their origin: Moderate absorption rate of *Coula edulis* shells: The polar shell of *Coula*

edulis has a lower absorption compared to both species of *Cocos nucifera*. The equatorial origin of *Coula edulis* shows a slightly higher absorption (18.47%) but remains lower than that of *Cocos nucifera* (species 2). Influence of location (Polar vs. Equatorial): The variation in absorption may be related to structural differences in the shells depending on their region of origin. These differences include: Shell porosity. Chemical composition (lignin content, cellulose, etc.). Ambient humidity or local environmental conditions. Positioning relative to *Cocos nucifera*: *Cocos nucifera* shells have a higher absorption rate, suggesting a more porous structure or a higher affinity for water. This may be due to their more hydrophilic chemical composition. The work of Ganou *et al.* (2020) [33] confirms that *Cocos nucifera* shells (20.42%) have a higher absorption capacity, probably due to their lighter texture and increased porosity. The results for *Coula edulis* are in line with studies showing that denser and more compact shells, such as those of tropical nuts, have lower absorption, but better mechanical resistance. Direct comparison: *Coula edulis* shells are less absorbent than *Cocos nucifera* shells. This indicates a potentially denser and less permeable structure. *Coula edulis* shells could be more suitable for applications requiring low absorption (insulation, composite materials), while *Cocos nucifera* could be suitable for uses where water interaction is beneficial. Analyse in detail the chemical composition and structural properties of the shells to explain the variations and extend the comparisons to other tropical species.

3.1.3. Study of Porosity

The determination of the apparent density yielded an average value of 0.925 g/cm^3 for the equatorial zone and 0.859 g/cm^3 for the polar zone (**Figure 13(a)**). The values obtained are lower than those of certain shells known in the literature, notably coconut shells (Nucifera) from Cameroon (1.49 g/cm^3) and the kernels of *Canarium schweinfurthii* (1.46 g/cm^3) [33]. Similarly, the determination of the real density yielded an average value of 0.998 g/cm^3 for the equatorial zone and 0.901 g/cm^3 for the polar zone (**Figure 13(b)**). These results show that the polar zone has a lower density than the equatorial zone.

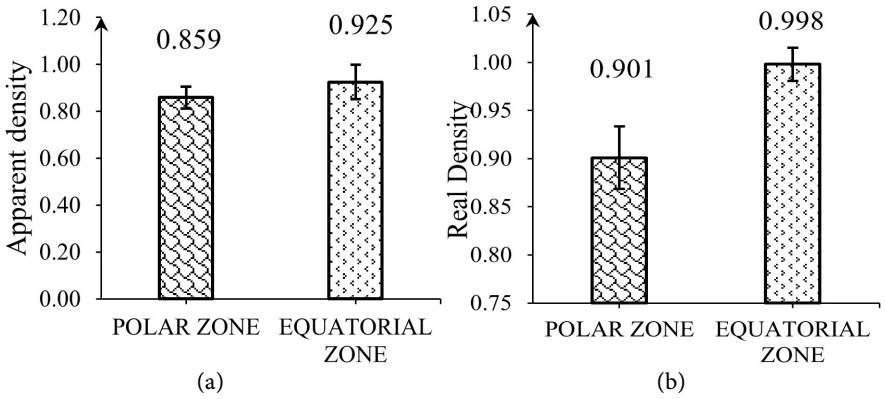

Figure 13. Density distribution: (a) Apparent density distribution. (b) Real density distribution.

The results obtained from the porosity give 7.35% for the equatorial zone and 4.61% for the polar zone. The polar zone has a lower porosity compared to the equatorial zone. This suggests that the shells from the polar zone have a more compact structure and less internal void. The higher porosity may indicate a looser internal structure or an increased presence of microcracks in the shell. The shells from the polar zone, with lower porosity, could have better mechanical strength and be more suitable for applications requiring dense materials. The shells from the equatorial zone, with higher porosity, could be lighter and have better thermal insulation capabilities. The shells of *Coula edulis* have an intermediate porosity compared to other tropical shells, making them versatile for various industrial applications. Previous studies on other shells, such as *Cocos nucifera*, show generally higher porosity (often above 10%) [33] [47], confirming that *Coula edulis* is a dense and strong raw material. These unique properties could be explored for specific applications, such as the manufacture of composite materials or absorbents.

3.2. Chemical and Thermal Analysis

3.2.1. Analysis of Fourier Transform Infrared Spectrometry (FTIR)

The FTIR analysis is in **Figure 14** shows that the functional groups of the shell of "*Coula edulis*" are identical regardless of the zone of the shell where the samples are taken. The peak at 3438 cm^{-1} observed on the curves is caused by the variation in O-H stretching and hydrogen bonding of the hydrogen group [48]. The two peaks at 3000 cm^{-1} and 2900 cm^{-1} are the characteristic bands of the stretching variation of C-H, CH, and CH2 in cellulose and hemicellulose. The peak at 1736 cm^{-1} can be attributed to the carboxylic group CO, which corresponds to the variation of carboxylic acid in lignin [49].

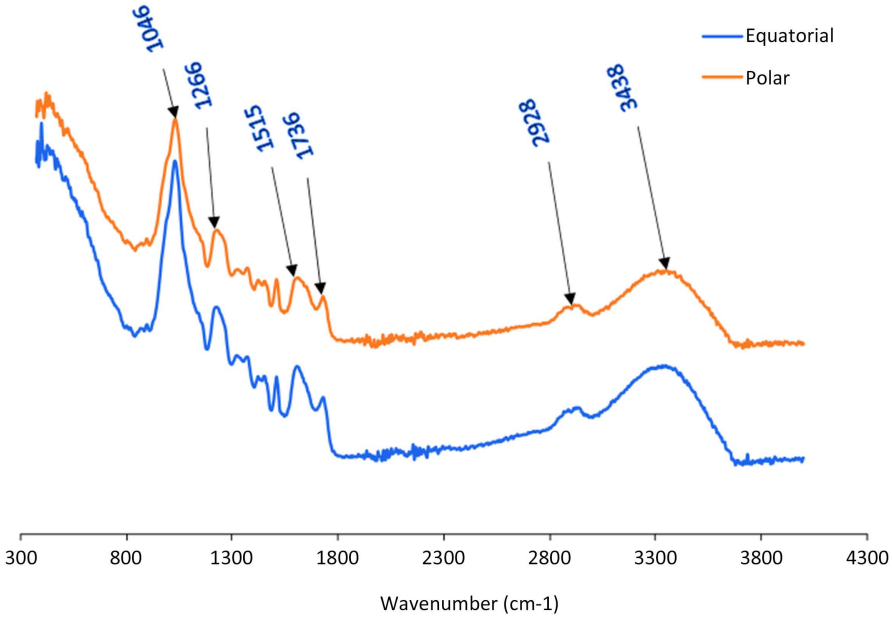

Figure 14. FTIR spectrum.

However, we observe a highlighting by the decrease of the characteristic absorbance signal at the peak of 1736 cm^{-1} which corresponds to the symmetrical extension of the C=O of hemicelluloses and pectins. While the peak at 1515 cm^{-1} is attributed to the C-C stretching of the aromatic ring of lignin. The two peaks at 1500 cm^{-1} and 1293 cm^{-1} were also observed, which correspond to the shearing of the C-H and C-O bond of the aromatic ring in free water [50]. The absorbance peak centered at 1266 cm^{-1} is due to the C-O stretching vibration of acetyl grouped in lignin [51]. The peaks at 1200 cm^{-1} and 1085 cm^{-1} are associated with the stretching vibrations of C-O-C and C-O of the hydroxide and ether group in cellulose. The peak at 1049 cm^{-1} can be attributed to the presence of glycosuric bonds, while the peak at 560 cm^{-1} corresponds to the C-OH bending [51]. The different peaks observed make it possible to say that "*Coula edulis*" is a lignocellulosic material with a varied presence of several functional groups within the material.

3.2.2. Thermogravimetric Analysis (TGA)

Figure 15 shows the Thermogravimetric curves TG and its Derivatives DTG. The analysis of the ATG curve shows that the weight loss as a function of the temperature of "*Coula edulis*" shells is similar to that of other plant by-products such as wood [36]. It is noted that there are four degradation phases on this TGA thermogram, the first phase is attributed to dehydration (evaporation of moisture) caused by the hydrophilic nature of lignocellulosic materials [52], with a weight loss of 7.222% occurring between 30˚C and 80˚C.

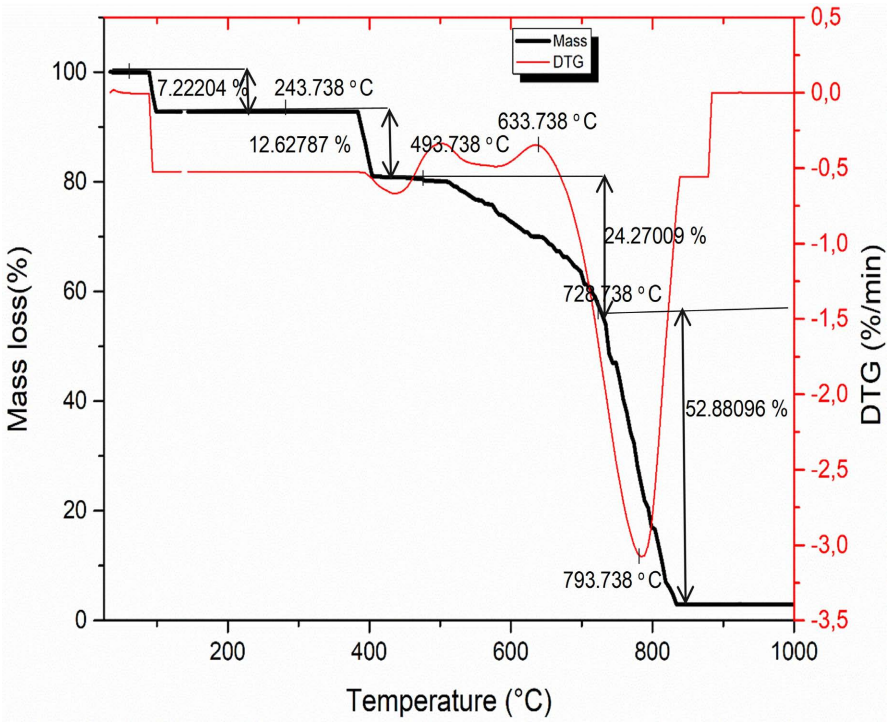

Figure 15. Thermogravimetric analysis curves of the *Coula edulis* shells.

The second phase occurs between 80˚C and 395˚C with a higher weight loss of 12.627% this loss corresponds to the decomposition of hemicellulose and a small amount of cellulose. The third phase of degradation which is recorded between 493˚C and 728˚C is the loss of the elements constituting the shell such as cellulose, hemicellulose, lignin, and pectins [53]. In the fourth phase between 729˚C and 842˚C then from 842˚C to 1000˚C, with a weight loss of 52.88096%, the shell is reduced to ash [52]. This analysis makes it possible to position "*Coula edulis*" as an aggregate of choice for the production of eco-materials that can withstand high temperatures (approximately 500˚C - 800˚C). The study revealed that these shells exhibit significant thermal stability, superior to some commonly used thermoplastic materials. In comparison with some shells [36], (*Coconut nucifera*, and *Canarium kernels*) contain about 82% volatile matter, 16% fixed carbon, and less than 3% ash. This result is close to that of other studies previously conducted in the literature by doing the thermal analysis of other plant shells [36].

3.2.3. X-Ray diffraction (XRD)

The analysis of the DRX curve shows in **Figure 16**, a main peak (high intensity around 30˚): This peak corresponds to the presence of calcite ($CaCO_3$), a major crystalline form often observed in lignocellulosic shells and organic materials containing carbonates. [52]. Secondary peaks are observed between 20˚ and 50˚: They indicate the presence of minor crystalline phases, probably linked to elements such as quartz (SiO_2), kaolinite (K), or other metal oxides such as magnesium or aluminum. Annotations such as Q (Quartz), K (Kaolinite) and other identified materials (e.g. Co for Carbonates, He for Hematite) reinforce this hypothesis [53]. The predominant crystalline structure: The dominance of calcite and the presence of quartz are classic characteristics of lignocellulosic shells, due to their organo-mineral composition. Calcite plays a role in the mechanical rigidity and strength of the shells. Presence of amorphous phases: A relatively low intensity between certain diffraction angles could indicate an amorphous portion, related to the cellulose or hemicellulose of the shells. If two samples are compared (polar vs. equatorial), minor differences in peak intensity may reflect variations in density or chemical composition between these areas. Consistency with lignocellulosic materials: The presence of calcite and quartz is consistent with other studies on similar shells (e.g. *Cocos nucifera*), where similar crystal structures have been identified [54]. This crystal composition indicates that the shells of "*Coula edulis*" could be used as mineral fillers in composite materials or as absorbents due to their porous and crystalline structure. [55]. The X-ray diffraction curve of the "*Coula edulis*" shells reveal a mainly crystalline structure, dominated by calcite and quartz, with amorphous phases associated with organic constituents [56]. These results are in line with existing literature and confirm their potential for industrial applications, particularly in the field of materials or water treatment. **Figure 16** shows the representation of X-ray diffraction.

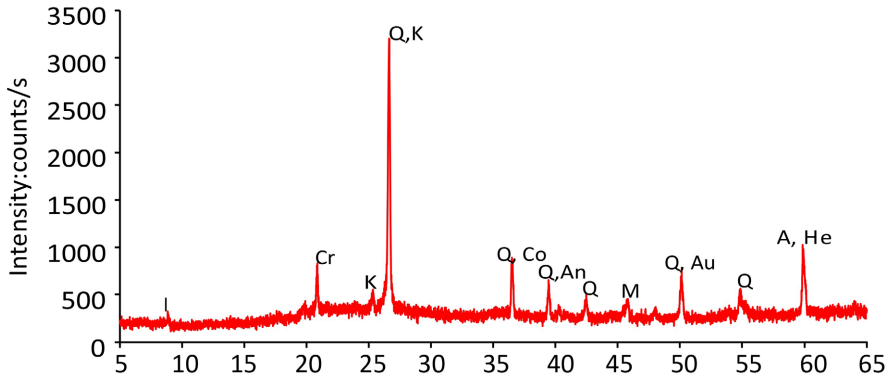

Figure 16. XRD Analyses Cuves of *Coula edulis* Shell.

A study of chemical transformations during drying reveals the thermal degradation of organic components: At certain temperatures, lignin, cellulose, and hemicellulose can decompose differently, affecting the rigidity and drying capacity of the shells. A thermogravimetric analysis (TGA) allowed us to measure these mass losses. The modification of the chemical composition by infrared spectroscopy (FTIR). As well as the X-ray diffraction (XRD). If some models work better, it is perhaps because they take into account specific phenomena (internal diffusion, surface resistance, convection). The statistical comparison (correlation coefficient R^2, mean error RMSE) would allow us to identify the most suitable models. By comparing the data obtained for *Coula edulis* with those of other similar biomaterials (coconut shells, palm nut shells) [36], we better understand the physical and chemical particularities of the shells influencing their behavior during drying. Explanations of the differences in performance between the models could be addressed by further analyses of physical structure, chemical composition, and modeling. Given the different characteristics, *Coula edulis* shells have several interesting properties, such as their thermal stability, and their richness in carbon. These characteristics make them suitable for various industrial applications: For biocomposite materials, as reinforcement of plastics and polymers. The crushed shells can be incorporated into composite materials to improve their mechanical resistance and durability. Alternatives to mineral fillers (silica, talc), They can partially replace synthetic fillers in biodegradable plastics and ecological composites. In the production of activated carbon and adsorbent materials. The shells can also be transformed into granules or briquettes for industrial and domestic heating. In the abrasives and technical surfaces industry, for the manufacture of natural abrasives, crushed shells can be used as soft abrasives in industrial cleaning and preparation of metal surfaces. As Finishing and polishing, the shells can be used for polishing metals and sensitive electronic components. In building materials, shells can be incorporated as aggregates in concrete formulations to improve thermal and acoustic insulation. Also, as fillers in ecological building panels.

4. Conclusion

In this work, the aim was to evaluate the physical, chemical, and thermal cha-

racteristics of African hazelnut shells "*Coula edulis*". To do this, two sampling zones and four isotherms (60˚C, 75˚C, 90˚C, 105˚C) were taken into account for physical tests. This allowed the determination of the relative humidity rate (RHR), the diffusion coefficient, and the activation energy. The results from the drying study obtained gave an RHR of 16.05% for the polar zone and 13.38% for the equatorial zone. The diffusion coefficient obtained is $1.21 \times 10^{-7} \pm 1.20 \times 10^{-8}$% to $2.35 \times 10^{-7} \pm 1.17 \times 10^{-8}$% and $3.07 \times 10^{-8} \pm 2.49 \times 10^{-9}$% to $4.82 \times 10^{-8} \pm 4.89 \times 10^{-9}$% for the polar zone. As for the equatorial zone it varies from $1.24 \times 10^{-7} \pm 9.84 \times 10^{-9}$% to $1.52 \times 10^{-7} \pm 1.28 \times 10^{-8}$% and from $3.26 \times 10^{-8} \pm 3.24 \times 10^{-9}$% to $3.86 \times 10^{-8} \pm 3.27 \times 10^{-9}$%. The activation energy values were 9.924 kJ/mol for the polar zone and 3.917 kJ/mol for the equatorial zone. The absorption rate of the polar zone is 16.32 ± 3.20% and that of the equatorial zone is 18.47 ± 2.04%, with a porosity rate of 7.357% in the equatorial zone and 4.611% in the polar zone. The Newton and Lewis model very well satisfies the experimental data of drying kinetics. Among the 05 models tested in absorption, the Page model is the one that offers the best correlation compared to the Gowen and Sikame models. It also appears that the adsorption kinetics are almost identical in both zones. The Fourier Transform Infrared Spectroscopy (FTIR) analysis showed a similarity in the spectra. Thermogravimetric Analysis (TGA) and X-ray Diffraction (XRD) show that the shells of "*Coula edulis*" have a structure similar to that of wood materials and other hard-shelled plants. These various tests have made it possible to understand the theory of water diffusion in the shells of "*Coula edulis*", Following this work, several short-term perspectives can be considered regarding the shells of "*Coula edulis*" and a bio-composite: The mechanical characterization of hazelnut shells to determine the hardness, Young's modulus, and the creep rate.

Conflicts of Interest

The authors declare no conflicts of interest regarding the publication of this paper.

References

[1] Antwi-Boasiako, C. and Glalah, M. (2021) Physico-Combustion Characteristics and Suitability of Six Carbonized Tropical Hardwoods as Biofuels for Domestic and Industrial Applications. *Biomass and Bioenergy*, **153**, Article 106208. https://doi.org/10.1016/j.biombioe.2021.106208

[2] Fotang, C., Dutton, P., Bröring, U., Roos, C., Willie, J., Angwafo, T.E., *et al.* (2023) Tool Use by Nigeria-Cameroon Chimpanzees for Driver Ant Predation in Kom-Wum Forest Reserve, North-West Region Cameroon. *Folia Primatologica*, **94**, 73-85. https://doi.org/10.1163/14219980-bja10006

[3] Zam, J.F., Biwole, A.B., Eyinga, J.J.B., Fongnzossie, E.F., Bessike, G.J., Mouangue, R., *et al.* (2024) Determining the Quality of Wood Charcoals as a Bioenergy Source in Humid Tropical Regions of Central Africa: The Effect of Carbonized Wood and Storage Time. *Biomass Conversion and Biorefinery*, **15**, 6971-6987. https://doi.org/10.1007/s13399-024-05763-3

[4] Kamdem, N.G., Sergeant, S., Vercruysse, C., Deblauwe, V., Sonké, B. and Hardy, O.J. (2024) Development and Characterization of Nuclear Microsatellite Markers for the

African Walnut *Coula edulis* Baill (*Coulaceae*). *Molecular Biology Reports*, **51**, Article No. 438. https://doi.org/10.1007/s11033-024-09373-0

[5] Yves, O., Josiane, E.Y., Latran, O.J.P., Michel, E. and Didace, M.T.M. (2024) Study of the Nutritional Value of *Coula edulis* Kernels from Sembé (Republic of Congo). *International Journal of Frontline Research in Science and Technology*, **3**, 1-7. https://doi.org/10.56355/ijfrst.2024.3.1.0042

[6] Josiah, N.E., Zudonu, O.C. and Onyeji, C.C. (2020) Phytochemical Analysis, Antioxidant and Antimicrobial Studies of Ethanol Extract of *Coula edulis* Seed Shell. *GSC Biological and Pharmaceutical Sciences*, **12**, 48-53. https://doi.org/10.30574/gscbps.2020.12.1.0056

[7] Kepawou, M.G., Akamba, B.D.A., Kamdem, M.H.K., Piebeng, C.Q.N., Chimeze, V.W.N., Ebouel, F.L.E., Mmutlane, E.M., Ndinteh, D.T., Mbazoa, C.D., Ngondi, J.L. and Wandji, J. (2024) Anti-Hyperglycemic Effect of Two Terpenoids Isolated from *Coula edulis* on Normoglycemic Rats and in Silico Study of Their Potential Inhibitors on A-Amylase and Dipeptidylpeptidase 4. *Journal of Drug Delivery and Therapeutics*, **14**, 147-157. https://doi.org/10.22270/jddt.v14i2.6406

[8] Bopenga, C.S.A.B., Degboevi, H.M., Candelier, K., Engonga, E.P., Dumarçay, S., Thévenon, M.F., Charbonnier, C.G. and Gérardin, P. (2021) Characterization of Extracts from the Bark of the Gabon Hazel Tree (*Coula edulis* Baill) for Antioxidant, Antifungal and Anti-Termite Products. *Journal of Renewable Materials*, **9**, 17-33. https://doi.org/10.32604/jrm.2021.013366

[9] Yoca, J.E., Ossoko, J.P.L., Okandza, Y. and Tsieri, M.D.M. (2024) Fatty Acid Composition of Hazelnut Kernel Oil from *Coula edulis* Collected in the Republic of Congo. *Food and Nutrition Sciences*, **15**, 290-297. https://doi.org/10.4236/fns.2024.154019

[10] Beyegue, E., Azantsa, B.G.K., Mbong, A.M. and Oben, J.E. (2021) Inhibition of Digestive Enzymes, Antioxidant and Free Radical Scavenging Capacities of Stem Bark Extracts of *Coula edulis* Baill (*Olacaceae*). *Journal of Food Research*, **10**, 1-17. https://doi.org/10.5539/jfr.v10n5p1

[11] Jana, U.K. and Patra, K.K. (2024) Seasonal Variations in the Antioxidant and Phytochemical Composition of Five Wild Edible Plants from Paschim Medinipur: Implications for Nutritional Value. *International Journal for Multidisciplinary Research*, **6**, 1-3. https://doi.org/10.36948/ijfmr.2024.v06i01.12070

[12] Moupela, C., Doucet, J., Daïnou, K., Meunier, Q., Vermeulen, C. and Beauchêne, J. (2013) Essais de propagation par semis et marcottage aérien de *Coula edulis* Baill. et perspectives pour sa domestication. *Bois & Forets des Tropiques*, **318**, 3-13. https://doi.org/10.19182/bft2013.318.a20516

[13] Clark, J. and Linares-Matás, G. (2023) Seasonal Resource Categorization and Behavioral Adaptation among Chimpanzees: Implications for Early Hominin Carnivory. *Journal of Anthropological Sciences*, **101**, 1-35.

[14] Janani, S., Kulanthaivel, P., Sowndarya, G., Srivishnu, H. and Shanjayvel, P.G. (2022) Study of Coconut Shell as Coarse Aggregate in Light Weight Concrete—A Review. *Materials Today: Proceedings*, **65**, 2003-2006. https://doi.org/10.1016/j.matpr.2022.05.329

[15] Koops, K., Akankwasa, W., Camara, H.D., Fitzgerald, M., Keir, A., Mamy, G., *et al.* (2024) Flexible Grouping Patterns in a Western and Eastern Chimpanzee Community. *American Journal of Primatology*, **86**, e23593. https://doi.org/10.1002/ajp.23593

[16] Wang, Z., Yan, J., Pawley, M., Brunton, D.H., Qu, J., Grueter, C.C., *et al.* (2024) Do

Degraded Grasslands Provide a Better Habitat for Plateau Pika?—Testing the Nutritional Hypothesis. *Agriculture, Ecosystems & Environment*, **367**, Article 108993. https://doi.org/10.1016/j.agee.2024.108993

[17] Ekissi, G.S.E., Tanoh, K.M., Fagbohoun, B.J., Yapi, J.C. and Kouame, P.L. (2019) Physical Parameters of African Hazelnut (*Coula edulis* B.) and Effect of Cooking Time on Physicochemical Properties. *Scholars International Journal of Chemistry and Material Sciences*, **2**, 23-30.

[18] Balogoun, C., Bawa, M., Osseni, S. and Aina, M. (2015) Préparation des charbons actifs par voie chimique à l'acide phosphorique à base de coque de noix de coco. *International Journal of Biological and Chemical Sciences*, **9**, 563-580. https://doi.org/10.4314/ijbcs.v9i1.48

[19] Douh, C., Malonga, L.M., N'zala, D., Mabengo, B.C., Moussoumbou, C., Ndzaï, S.F., *et al.* (2023) Regeneration Potential of Woody Species at the Side of Secondary Roads Post-Logging of Loundoungou-Toukoulaka Forest Management Unit, Republic of the Congo. *Natural Resources*, **14**, 102-120. https://doi.org/10.4236/nr.2023.147008

[20] Offiong, E. and O Otu, D. (2023) Evaluation of Timber Trees Producing Valuable Fruits and Seeds in Cross River State. *Global Journal of Agricultural Sciences*, **22**, 1-5. https://doi.org/10.4314/gjass.v22i1.1

[21] Andika, R., Arinana, A., Sari, R.K., Rahmawati, A.I. and Himmi, S.K. (2025) Antitermite Activity of Eucalyptus Pellita Bark Extract. *Jurnal Sylva Lestari*, **13**, 32-44. https://doi.org/10.23960/jsl.v13i1.1023

[22] García Carrasco, J. and Donoso González, M. (2022) Al alba de la humanización: Cultura proyecta sombra de poliedro, género de mujer y práctica de magisterio. *Revista Española de Pedagogía*, **80**, 251-267. https://doi.org/10.22550/rep80-2-2022-05

[23] Ntinkam, C.A., Dika, J.M. and Kede, C.M. (2024) Green Synthesis and Physicochemical Characterization of an Eco-Friendly Zero-Valent Iron Biochar Based on *Coula edulis* Shell. *Materials Advances*, **6**, 184-195.

[24] Steven, S., Pasymi, P., Hernowo, P., Restiawaty, E. and Bindar, Y. (2023) Investigation of Rice Husk Semi-Continuous Combustion in Suspension Furnace to Produce Amorphous Silica in Ash. *Biomass Conversion and Biorefinery*, **14**, 25757-25772. https://doi.org/10.1007/s13399-023-04777-7

[25] Olatunji, K.O., Mootswi, K.D., Olatunji, O.O., Zwane, M.I., van Rensburg, N.J. and Madyira, D.M. (2025) Anaerobic Co-Digestion of Food Waste and Groundnut Shells: Synergistic Impact Assessment and Kinetic Modeling. *Waste and Biomass Valorization*. https://doi.org/10.1007/s12649-025-02904-1

[26] Yobo, C.M., Awono, A. and Ingram, V. (2020) Understanding the *Coula edulis*, *Dacryodes buettneri* and *Irvingia gabonensis* Non-Timber Forest Product Value Chains from Makokou, North-East Gabon from a Gender Perspective. *International Forestry Review*, **22**, 339-353. https://doi.org/10.1505/146554820830405672

[27] Barrera Hernandez, J.C., Sagastume Gutierrez, A., Ramírez-Contreras, N.E., Cabello Eras, J.J., García-Nunez, J.A., Barrera Agudelo, O.R., *et al.* (2024) Biomass-Based Energy Potential from the Oil Palm Agroindustry in Colombia: A Path to Low Carbon Energy Transition. *Journal of Cleaner Production*, **449**, Article 141808. https://doi.org/10.1016/j.jclepro.2024.141808

[28] Madhiyanon, T., Phila, A. and Soponronnarit, S. (2009) Models of Fluidized Bed Drying for Thin-Layer Chopped Coconut. *Applied Thermal Engineering*, **29**, 2849-2854. https://doi.org/10.1016/j.applthermaleng.2009.02.003

[29] Isa, J. and Jimoh, K.A. (2021) Mathematical Modelling of Drying Characteristics of Coconut Slices. *Turkish Journal of Agricultural Engineering Research*, **2**, 363-375. https://doi.org/10.46592/turkager.2021.v02i02.010

[30] Sahari, Y., Anuar, M.S., Mohd Nor, M.Z., Abdul Ghani, N.H. and Mohd Tahir, S. (2023) Progress, Trends and Development of Drying Studies on Coconut Kernel Products: A Review. *Pertanika Journal of Science and Technology*, **31**, 2621-2644. https://doi.org/10.47836/pjst.31.5.30

[31] Ndapeu, D., Njeugna, E., Bistac, S.B., Drean, J.Y., Fogue, M. and Foba, J.N. (2013) Experimental Study of the Drying Kinetics of the Coconut Shells (Nucifera) of Cameroon. *Materials Sciences and Applications*, **4**, 822-830. https://doi.org/10.4236/msa.2013.412105

[32] Ndapeu, D., Njeugna, E., Sikame, N.R., Bistac, S.B., Drean, J.Y. and Fogue, M. (2016) Experimental Study of the Water Absorption Kinetics of the Coconut Shells (Nucifera) of Cameroun. *Materials Sciences and Applications*, **07**, 159-170. https://doi.org/10.4236/msa.2016.73016

[33] Koungang, B.M.G., Ndapeu, D., Tchemou, G., Mejouyo, P.W.H., Ntcheping, B.W., Foba, J.T., *et al.* (2020) Physical, Water Diffusion and Micro-Structural Analysis of "*Canarium schweinfurthii* Engl". *Materials Sciences and Applications*, **11**, 626-643. https://doi.org/10.4236/msa.2020.119042

[34] Parisi, S., Parisi, C. and Varghese, S.M. (2024) Value Addition and Coconut-Based Beverages: Current Perspectives. *Beverages*, **10**, 14. https://doi.org/10.3390/beverages10010014

[35] Defo, N., Sikame, R.N.T., Huisken, W.P.M., Ndapeu, D., Tido, S.T., Bistac-Brogly, S., *et al.* (2023) Development and Characterization of Agglomerated Abrasives Based on Agro-Industrial By-Products. *Journal of Natural Fibers*, **20**, Article 2178579. https://doi.org/10.1080/15440478.2023.2178579

[36] Defo, N., Harzallah, O., Nicodème Tagne Sikame, R., Njeugna, E. and Bistac, S. (2024) Effect of Alkaline Treatment on Hard Vegetable Shells on the Properties of Biobased Abrasive Wheels. *Composites Part A*: *Applied Science and Manufacturing*, **184**, Article 108278. https://doi.org/10.1016/j.compositesa.2024.108278

[37] Zue, M., Mekui, M. and Eba, F. and Ondo A. (2020) Study of the Adsorption Equilibrium of Methylene Blue from Aqueous Solution onto Activated Carbon of Coulaedulis Nut Shells. *Research Journal of Chemistry and Environment*, **12**, 40-50.

[38] Beyegue, E., Youovop, J.F., Takuissu, G.R., Ndoue, N.E., Mbappe, F.E., Edou, F., *et al.* (2023) Acute and Sub-Chronic Toxicity Evaluation of the Ethanolic Extract of *Coula edulis* B., (*Olacaceae*) Stem Bark. *Asian Journal of Research in Medical and Pharmaceutical Sciences*, **12**, 156-172. https://doi.org/10.9734/ajrimps/2023/v12i4239

[39] Libog, L., Biyeme, F., Betené, A.D.O., Biwolé, A.B., Ndiwe, B., Mbang, J.P.E., *et al.* (2023) Influence of the Extraction Location on the Physical and Mechanical Properties of the Pseudo-Trunk Banana Fibers. *Journal of Natural Fibers*, **20**, Article 2204451. https://doi.org/10.1080/15440478.2023.2204451

[40] Mbou Tiaya, E., Huisken Mejouyo, P.W., Ndema Ewane, P.A., Damfeu, C., Meukam, P. and Njeugna, E. (2023) Effect of Particle Sizes on Physical, Thermal and Mechanical Behavior of a Hybrid Composite with Polymer Matrix with Raffia Vinifera Cork and Bambusa Vulgaris. *Polymer Bulletin*, **81**, 275-295. https://doi.org/10.1007/s00289-023-04702-y

[41] Meziane, S. (2013) Modélisation de la cinétique du séchage convectif du grignon d'olive. *Journal of Renewable Energies*, **16**, 379-387.

https://doi.org/10.54966/jreen.v16i2.387

[42] Fufa, D.D., Bekele, T., Tamene, A. and Bultosa, G. (2025) Drying Kinetic Models, Thermodynamics, Physicochemical Qualities, and Bioactive Compounds of Avocado (*Persea americana* Mill. Hass Variety) Seeds Dried Using Various Drying Methods. *Heliyon*, **11**, e41058. https://doi.org/10.1016/j.heliyon.2024.e41058

[43] Singh, S., Kawade, S., Dhar, A. and Powar, S. (2022) Analysis of Mango Drying Methods and Effect of Blanching Process Based on Energy Consumption, Drying Time Using Multi-Criteria Decision-Making. *Cleaner Engineering and Technology*, **8**, Article 100500. https://doi.org/10.1016/j.clet.2022.100500

[44] Daud, N.F.S., Mohd Said, F., Mohd Mohyiddin, I., Sy Mohamad, S.F., Md Zin, N.H., Ahmad Zakil, F., *et al.* (2024) Investigating the Impact of Blanching and Salt Treatment on the Drying Kinetics of Oyster Mushrooms. *Bioresource Technology Reports*, **27**, Article 101943. https://doi.org/10.1016/j.biteb.2024.101943

[45] Nimjieu, H.T., Rodrigue, S.T.N., Roussel, N.T.P., William, H.M.P., Stanislas, T.T., Medard, F., *et al.* (2023) Analytical and Numerical Investigation of Water Diffusion through Raffia Vinifera Pith. *Journal of Natural Fibers*, **20**, Article 2164105. https://doi.org/10.1080/15440478.2022.2164105

[46] Takoumbe, C., Zobo Mfomo, J., Biwole, A.B., Mbou Tiaya, E., Mono, J.A., Pokem Nguimjeu, P.H., *et al.* (2024) Effect of Reinforcement Ratio and Particle Size on the Physical and Mechanical Performance of Epoxy Matrix Panels and Waste Wood from Iroko *Chlorophora excelsa* from Cameroon. *Advances in Materials Science and Engineering*, **2024**, Article ID: 9915731. https://doi.org/10.1155/2024/9915731

[47] Mejouyo, P.W.H., Harzallah, O., Tagne, N.R.S., Ndapeu, D., Tchemou, G., Drean, J.Y., *et al.* (2021) Physical and Mechanical Characterization of Several Varieties of Oil Palm Mesocarp Fibers Using Different Cross-Sectional Assumptions. *Journal of Natural Fibers*, **18**, 175-191. https://doi.org/10.1080/15440478.2019.1612813

[48] Youbi, S.B.T., Tagne, N.R.S., Harzallah, O., Huisken, P.W.M., Stanislas, T.T., Njeugna, E., *et al.* (2022) Effect of Alkali and Silane Treatments on the Surface Energy and Mechanical Performances of *Raphia vinifera* Fibres. *Industrial Crops and Products*, **190**, Article 115854. https://doi.org/10.1016/j.indcrop.2022.115854

[49] Chattaraj, S., Samantaray, A., Ganguly, A. and Thatoi, H. (2025) Employing Plant Growth-Promoting Rhizobacteria for Abiotic Stress Mitigation in Plants: With a Focus on Drought Stress. *Discover Applied Sciences*, **7**, Article No. 68. https://doi.org/10.1007/s42452-025-06468-6

[50] Ella Nkogo, L., Mikala Mouendou, M.S., Dumarçay, S., Edou Engonga, P. and Gérardin, P. (2024) Phytochemical Study, FTIR and GC-MS Characterization and Evaluation of the Antioxidant Activity of *Letestua durissima* Extracts. *Forests*, **15**, Article 429. https://doi.org/10.3390/f15030429

[51] Ni, Z., Song, Z., Bi, H., Jiang, C., Sun, H., Qiu, Z., *et al.* (2023) The Effect of Cellulose on the Combustion Characteristics of Coal Slime: TG-FTIR, Principal Component Analysis, and 2D-COS. *Fuel*, **333**, Article 126310. https://doi.org/10.1016/j.fuel.2022.126310

[52] Li, J., Gao, J., Fang, J., Ling, T., Xia, M., Cao, X., *et al.* (2023) Environmental-friendly Regenerated Lignocellulose Functionalized Cotton Fabric to Prepare Multi-Functional Degradable Membrane for Efficient Oil-Water Separation and Solar Seawater Desalination. *Scientific Reports*, **13**, Article No. 5251. https://doi.org/10.1038/s41598-023-32566-9

[53] Arromdee, P. and Ninduangdee, P. (2022) Combustion Characteristics of Pelletized-Biomass Fuels: A Thermogravimetric Analysis and Combustion Study in a Fluidized-

Bed Combustor. *Energy, Ecology and Environment*, **8**, 69-88. https://doi.org/10.1007/s40974-022-00263-4

[54] Taha, M.A., Gad, S.A. and Youness, R.A. (2025) Development of Fe/SiBr/Si_3N_4/silica Fume Nanocomposites from Recycled Metal Waste for Industrial Applications. *Scientific Reports*, **15**, Article No. 1529. https://doi.org/10.1038/s41598-024-81657-8

[55] Yang, T., Huang, B., Zhan, C., Jiang, C., Zhang, L., Zhao, X., *et al.* (2025) Mechanical Properties and Mechanisms of Soda Residue and Fly Ash Stabilized Soil. *Scientific Reports*, **15**, Article No. 1103. https://doi.org/10.1038/s41598-024-84170-0

[56] Zaidi, R., Khan, S.U., Farooqi, I.H., Ahmed, F., Alsulami, A., Azam, A., *et al.* (2025) Performance, Isotherm, Kinetics and Mechanism of Simultaneous Removal of Cr(VI), Cu(II) and F Ions by CeO_2-MgO Binary Oxide Nanomaterials. *Scientific Reports*, **15**, Article No. 1431. https://doi.org/10.1038/s41598-024-78830-4